IEEE Access
Multidisciplinary | Rapid Review | Open Access Journal

Received June 3, 2021, accepted June 20, 2021, date of publication July 2, 2021, date of current version July 12, 2021.

Digital Object Identifier 10.1109/ACCESS.2021.3094172

Reduction of Torsional Vibrations Excited by Electromechanical Interactions in More Electric Systems

CONSTANZA AHUMADA[1], (Member, IEEE), AND PATRICK WHEELER[2], (Fellow, IEEE)
[1]Department of Electrical Engineering, University of Chile, Santiago 8370448, Chile
[2]Department of Electrical and Electronic Engineering, University of Nottingham, Nottingham NG6 2RD, U.K.

Corresponding author: Constanza Ahumada (coahumad@uchile.cl)

This work was supported in part by the University of Chile U-Inicia under Grant UI-030/19, and in part by the Fondo Nacional de Desarrollo Científico y Tecnológico (FONDECYT) Iniciación under Grant N°11200866.

ABSTRACT This paper studies the excitation of torsional vibrations by electromechanical interaction after the connection of electrical loads. Electrical generation and power system in aircraft are becoming of key importance, especially considering the current roadmap for aerospace systems' electrification. However, since the drivetrain which links electrical generators to the main engine is relatively flexible in most aircraft structures, torsional vibrations can be excited by the sudden connection or disconnection of electrical loads, thus increasing the drivetrain's fatigue and reducing its reliability and lifetime. Because of the increased amounts of intermittent electrical loads on aircraft systems, which excite torsional vibrations through electromechanical interactions, the electrical load connections are investigated in this paper. Specifically, a method for reducing torsional vibrations in aircraft drivetrains is proposed to extend their lifespan. This method is applied directly to the load being connected and it proposes the connection of the electrical loads following a pulsating pattern, for which the pulse connection time is determined as a function of the drivetrain vibration modes. Simulations results show that the proposed method provides a significant reduction in the drivetrain shaft torsional vibrations. Experimental results validate the simulation data showing the benefits this method can provide in drivetrain reliability, weight reduction and cost.

INDEX TERMS Aircraft power systems, aircraft propulsion, electromechanical effects, engines, more electric systems, vibration control.

I. INTRODUCTION

Air traffic is increasing at a rate of 4.8% per annum [1], producing 2% of anthropogenic CO_2 emissions [2] and, with the ongoing rise in passengers, it is estimated that this number will increase to 3% by 2050. To decrease the impact of the aerospace industry on the environment, the Advisory Council for Aeronautics Research in Europe (ACARE) has set targets for reducing CO_2 emissions of 75%, NO_x emissions of 90%, and acoustic pollution of 65%, respectively, by 2050 [2]. To achieve these goals and reduce the cost, aircraft's fuel efficiency must be improved.

A promising solution for reducing emissions is using more electric systems, such as the More Electric Aircraft (MEA). MEA technology aims to replace the pneumatic, hydraulic, and mechanical systems with electrical ones, reducing weight and fuel consumption [3], [4]. Consequently, the Electrical Power System (EPS) of MEA is considerably larger than in a traditional aircraft, bringing new challenges to the system design. In particular, MEA electrical loads are often high-power transient or pulsating loads [4], [5]. For example, solid-state phased-array radar loads, which typically require up to 30 kW at a voltage such as 10 V_{dc}, are pulsed and have stringent ripple requirements [6]. Moreover, in B787, loads traditionally supplied by the pneumatic system are now electrical driven. These loads include wing ice protection system (IPS), environmental control system (ECS), and engine starting system [7].

Fig. 1 shows a schematic connection of these electrical loads. The aircraft engine is connected through a drivetrain

The associate editor coordinating the review of this manuscript and approving it for publication was Hassen Ouakad.

to an electrical generator that supplies the EPS, including high-power transient or pulsating loads. One of the main issues with this configuration is that, since the generator shaft is designed to be flexible to reduce its weight, the aforementioned high-power or pulsating loads connection can cause mechanical vibrations in the system. In particular, the increased level of coupling between the EPS and the aircraft drivetrain excites torsional vibrations or twisting of the shafts on their axis on the drivetrain shaft. These vibrations can ultimately damage the drivetrain because of the cumulative effects of vibrations over time, leading to fatigue of the material [8], [9].

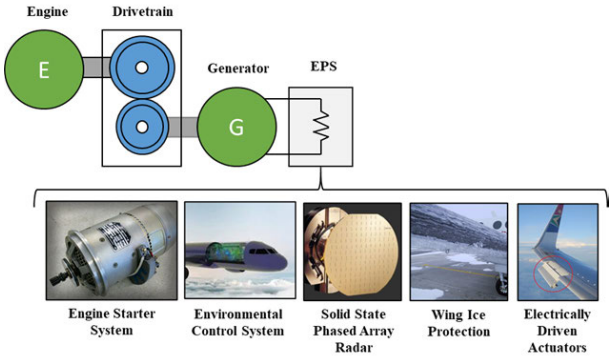

FIGURE 1. Electromechanical system schematic.

This phenomenon, known as electromechanical interaction, has been analyzed for aircraft engine systems in [8], [9]. These works identify the aircraft drivetrain natural frequencies, propose reduced models of the aircraft electromechanical interactions, and show that the connection of electrical loads can excite torsional vibrations in the engine's drivetrain. The reduction of the torsional vibrations excited by electromechanical interaction was discussed in [10], it was shown that ramping the torque can reduce the vibrations excited. However, the optimal ramp slope value was not analyzed. Thus, the load connection or the machine torque control can take longer than needed, making the system unnecessarily slow. A theoretical analysis of the ramp slope can allow an optimal solution to be used. Therefore, the purpose of this paper is to propose, analyze, and experimentally validate new strategies for reducing torsional vibrations excited by load connections in aircraft systems.

In other applications, to reduce the electromechanical interactions, different approaches usually are considered. For systems with periodic excitation, such as a generic drive system, the drivetrain's natural frequencies and vibration modes are first identified [8], [11], [12]. The excitation of torsional vibrations is then avoided by operating the system at different frequency values. For systems where electrical loads' arbitrary switching produces electromechanical interactions, the system is usually designed to have higher damping or stiffness and hence move the mechanical frequencies outside the operating areas [13]. However, this solution cannot be used to aircraft systems, where weight and size reduction are important factors [8]. Other approaches suggest adjusting the speed control of the machine, using ramp speed control [14], [15] or applying filters and dampers to the speed control [16], [17]. For example, some strategies propose the use of closed-loop torque controllers using PI [16], [18], non-linear controllers [19], and adaptive and predictive control [20]. The main disadvantage of these methods is that they apply dampers to the mechanical system and they do not analyze the mechanical properties and thus they can take a longer time than needed. An alternative is the use of anti-resonant filters [18], [21]–[23] that cancel the excitation of torsional vibrations. In [24], a filter known as Posicast compensator or input-shaping control is described. Input-shaping is an open-loop control that defines an input profile that allows obtaining the desired output [25], [26]. When the torsional vibrations are excited by torque changes, the torque or load applied can be defined as a function of the vibrations' natural frequencies, which allows eliminating the excitation of the torsional frequencies after the load profile has been applied. The connection pattern can be carried out in half a period of the lowest drivetrain's natural frequency, making the connection faster than what is obtained with other control strategies. Input shaping strategies can be applied to any connection pattern, including switching pulses, multiple smaller step connections or ramps like the ones proposed in [15], allowing the application of an optimal ramp that suppresses the excitation of vibrations in a minimal time.

Additionally, most strategies used to reduce torsional vibrations independently of the source of the vibrations are implemented in the machine drive as an active damping control [14], [15], [17]. This paper proposes a different approach, which is focused on the source of the torsional vibrations. For this reason, the proposed Posicast control is implemented directly in the electrical loads, which excite the torsional vibrations when connecting and disconnecting. Since Posicast control can define any optimal input, in this paper, an optimal pulse, which can be applied directly on electrical loads of switching nature, such as IPS, is proposed. This control strategy removes the need for additional control components and can be integrated into the load connection, making the proposed control strategy safe to apply in aircraft applications.

The contributions of this paper are to:

- Propose and validate the use of a novel input-shaping strategy to reduce the excitation of torsional vibrations in aircraft applications.
- Describe a strategy to reduce the torsional vibrations excited by the connection of electrical loads, which is applied directly to the loads being connected. This allows the reduction of torsional vibrations without additional components or controllers, making it practical to apply.
- The reduction of torsional vibrations after the connection of electrical loads in aircraft applications is analyzed by simulation and validated experimentally using a reduced electromechanical system model.

The paper is organized as follows. Section II models the electromechanical system. In Section III, a theoretical analysis of the dynamic interaction between load connections and the system response is presented, and the strategy proposed to minimize the effects of torque impacts is described. In Section IV, simulation results are shown. In Section V, the control strategy is validated through experimental testing. Finally, in Section VI, conclusions are drawn, and the benefits of the proposed strategy are analyzed. that

II. MODELLING OF THE ELECTROMECHANICAL SYSTEM

The electromechanical interaction system must be studied and modelled to reduce the torsional vibrations excited by electrical loads. In this section, a reduced system with torsional vibration features similar to those of an aero-engine is described.

The electromechanical interaction model used in this paper was developed in [9] and, as shown in Fig. 2, it comprises the drivetrain (shafts and gearbox), generator and electrical loads. In the following two subsections, the mechanical and electrical systems are described in detail.

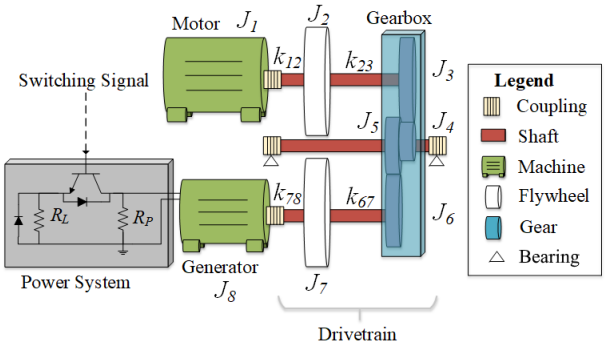

FIGURE 2. Electromechanical interaction system under study.

A. MECHANICAL SYSTEM MODEL

As presented in [9], an aircraft engine's drivetrain can be modelled by a reduced lumped mass system, in which loads, shafts, and the gearbox are modelled in terms of inertia, stiffness, and damping. Moreover, temperature and pressure do not affect the lower frequency torsional vibration modes, which are important in electromechanical interaction. Therefore, as shown in Fig. 2, the drivetrain model connects the engine spool to one generator through a gearbox with a motor/generator.

The drivetrain consists of three shafts rotating at different speeds, one connected to the prime mover, a middle shaft rotating faster, and one connected to the generator, as shown in Fig. 2. The central shaft is connected at both ends to a wall, and it is used for experiments out of the scope of this paper. The speed ratio between the three shafts is 1:3:1.5, with the motor shaft the slowest and the central shaft the fastest. The system is designed to have two vibrations modes below 100 Hz, representing the torsional vibrations features to those of the aircraft engine presented in [8].

The machines, gears, and flywheels are symbolized as inertia, while the couplings and shafts are characterized by stiffness and damping. The state of each inertia is given by:

$$J_i\ddot{\theta}_i = T_{i-1,i} - T_{i,i+1} \tag{1}$$

$$T_{i,i+1} = k_{i,i+1}(\theta_i - \theta_{i+1}) + d_{i,i+1}(\dot{\theta}_i - \dot{\theta}_{i+1}) \tag{2}$$

where J_i represent the inertia value referred to the generator shaft in kgm^2, θ_i, $\dot{\theta}_i$, $\ddot{\theta}$ are the angle in rad, the speed in rad/s, and the acceleration in rad/s^2 of the inertia, and $T_{i-1,i}$ and $T_{i,i+1}$ are the torque applied and transmitted by the inertia in Nm. The index i are given in Fig. 2. The torque applied by the engine, represented by a motor, is $T_{0,1} = T_m$. Instead, in the case of the generator $T_{8,9} = T_g$ is the electrical torque consumed by the machine. The rest of the torques on the system are proportional to the difference of speed and angle at each shaft and coupling ends and are given by (2). Finally, $k_{i,i+1}$ and $d_{i,i+1}$ represent the stiffness and damping of each shaft or coupling between inertias i and $i+1$ referred to the generator shaft. The complete lumped mass system is obtained applying (1) and (2) to the eight inertias representing the machines, flywheels, and gears, as shown in Fig. 2, resulting in the following system:

$$\mathbf{J}\ddot{\mathbf{x}} + \mathbf{D}\dot{\mathbf{x}} + \mathbf{K}\mathbf{x} = \mathbf{f}(t) \tag{3}$$

with

$$\mathbf{x} = \begin{bmatrix} \theta_1 \\ \theta_2 \\ \theta_6 \\ \theta_7 \\ \theta_8 \end{bmatrix} \quad \mathbf{f}(t) = \begin{bmatrix} T_m \\ 0 \\ 0 \\ 0 \\ T_e \end{bmatrix}$$

$$\mathbf{J} = \begin{bmatrix} J_1 & 0 & 0 & 0 & 0 \\ 0 & J_2 & 0 & 0 & 0 \\ 0 & 0 & J_{3,4,5,6} & 0 & 0 \\ 0 & 0 & 0 & J_7 & 0 \\ 0 & 0 & 0 & 0 & J_8 \end{bmatrix}$$

$$\mathbf{D} = \begin{bmatrix} d_{12} & -d_{12} & 0 & 0 & 0 \\ -d_{12} & d_{12}+d_{23} & -d_{23} & 0 & 0 \\ 0 & -d_{23} & d_{23}+d_{67} & -d_{67} & 0 \\ 0 & 0 & -d_{67} & d_{67}+d_{78} & -d_{78} \\ 0 & 0 & 0 & -d_{78} & d_{78} \end{bmatrix}$$

$$\mathbf{K} = \begin{bmatrix} k_{12} & -k_{12} & 0 & 0 & 0 \\ -k_{12} & k_{12}+k_{23} & -k_{23} & 0 & 0 \\ 0 & -k_{23} & k_{23}+k_{67} & -k_{67} & 0 \\ 0 & 0 & -k_{67} & k_{67}+k_{78} & -k_{78} \\ 0 & 0 & 0 & -k_{78} & k_{78} \end{bmatrix}$$

where $\mathbf{J}$ is the inertia matrix, $\mathbf{D}$ is the damping matrix, $\mathbf{K}$ is the stiffness matrix; $\mathbf{x}$ is the state of each element in the system, and $\mathbf{f}(t)$ is the excitation applied. Inertias 3-6 are combined to reduce the system, obtaining inertia $J_{3,4,5,6}$. It is important to highlight that the system described by (1)-(3) requires the knowledge of the mechanical system parameters, and it is used to study the system behaviour. In real aircraft applications, these parameters are usually known and

present minimal variations during operation [9]. Nevertheless, an estimation through an appropriate observer may be considered to improve the system knowledge [27].

B. ELECTRICAL SYSTEM MODEL

As presented in [9], the electrical system can be reduced from an AC three-phase to a DC electrical power system, since from the drivetrain and control perspective, the torque applied is equivalent. This reduction allows simplifying the building of the experimental setup while maintaining electromechanical interaction characteristics similar to the ones of the MEA and thus allowing the testing of the proposed control strategy.

The generator is represented by a DC machine with an independent winding connection, operating with constant field voltage. The output voltage is not controlled since it does not affect the control strategy applied. The machine electrical equations are given by

$$T_e = k i_f i_a \tag{4}$$

$$E = R_a i_a + L_a \frac{di_a}{dt} + V_0 + v_a \tag{5}$$

$$E = k i_f \omega_8 = k i_f \dot{\theta}_8 \tag{6}$$

$$v_a = R_{eq} i_a \tag{7}$$

in which T_e is the torque producing the electromotive force E, k is the back electromotive force constant equal to the torque constant, i_f is the field current, i_a is the armature current, v_a is the armature voltage, R_a and L_a are the armature resistance and inductance, V_0 is the voltage drop in the machine brushes, and ω_8 is the speed of the generator. R_{eq} is the total EPS resistive load obtained from $R_{eq} = (R_L R_P)/(R_L + R_P)$, where R_P and R_L are the resistance connected to the EPS, as shown in Fig. 2. The load resistance R_L can be connected or disconnected, thus changing the total load connected R_{eq}, by opportunely driving an Insulated-Gate Bipolar Transistor (IGBT), which is used as an ideal switch. The torque applied to the mechanical system T_g is given by:

$$T_g = T_e + T_w \tag{8}$$

where T_w is the torque consumed by the machine windage. Since the windage torque of the machine is usually much smaller than the torque applied to the mechanical system, T_g, the system can be approximated by assuming $T_g \approx T_e$. In this case, when operating with constant field current i_f, the torque applied to the mechanical system depends only on the armature current i_a which is proportional to the electrical load R_{eq} connected.

III. PROPOSED STRATEGY

This section describes the proposed input-shaping strategy, which reduces the excitation of torsional vibrations after electrical loads are connected. Posicast control defines an input signal for a given plant as a function of the plant natural frequencies, which allows obtaining the desired output [24]. Since input-shaping strategies depend on the system's plant, in this case, the aircraft mechanical drivetrain, next, the torsional vibrations excited by electromechanical interactions are described. After, the input-shaping strategy is proposed.

The mechanical model described by (3) is a linear time constant system. When a step connection $f(t)$ is applied to the system at rest, the system modal response can be described by the response of each vibration mode λ_j as given by

$$x(t) = \sum_{j=0}^{j=n} h_j e^{\lambda_j (t - T_k)} \tag{9}$$

$x(t)$ is the states' response; in this case, the angles of each inertia θ_j, T_k is the step connection time, and h_j is the step response of each vibration eigenvalue λ_j. A single step function will excite all modes of the system. If the system is subjected to m steps with sizes $p_1, p_2, \ldots, p_m$ at the times $T_1, T_2, \ldots, T_m$, the response of the system is the sum of the response to each step connection as given by

$$x(t) = \sum_{k=0}^{k=m} p_k \sum_{j=0}^{j=n} h_j e^{\lambda_j (t - T_k)} \tag{10}$$

The first vibration mode of the mechanical system is the rigid mode $\lambda_0 = 0$. Thus, (10) can be rewritten by

$$x(t) = h_0 p_0 + \sum_{j=1}^{j=n} h_j \sum_{k=1}^{k=m} p_k e^{\lambda_j (t - T_k)} \tag{11}$$

with $p_0 = \sum_{k=1}^{k=m} p_k$ the sum of all the steps being applied, which are constant. Therefore, $h_0 p_0$ represent the steady-state response of the system.

The undamped and underdamped torsional vibration modes studied in this paper can be modelled by the vibrations' frequency and damping. Therefore, the eigenvalues are complex conjugate pairs given by (12), where ω_{nj} is the natural frequency, ω_{dj} is the damped natural frequency, and ξ_j is the damping.

$$\lambda_j = \omega_{nj}(-\xi_j \pm j\sqrt{1 - \xi^2}) = -\xi_j \omega_{nj} \pm j\omega_{dj} \tag{12}$$

Since the exponential coefficient $\exp(\lambda_j(t - T_k)) = \exp((-\xi_j \omega_{nj} \pm j\omega_{dj})(t - T_k))$ has a real and imaginary component, to guarantee that the step response $h(t - T_k)$ is real, the coefficients h_j are also complex conjugate pairs. Now, the vibration modes eigenvalues λ_j and the step response h_j are separated in their real and imaginary parts, $\lambda_j = -\xi_j \omega_{nj} \pm j\omega_{dj}$ and $h_j = h_{jr} + j h_{jc}$ respectively, and equation (13) is found.

$$\begin{aligned} x(t) = p_0 h_0 + \sum_{j=1}^{n} [h_{jr} \sum_{k=1}^{m} [p_k e^{(-\xi_j \omega_{nj} + j\omega_{dj})(t - T_k)}] \\ + j h_{jc} \sum_{k=1}^{m} [p_k e^{(-\xi_j \omega_{nj} + j\omega_{dj})(t - T_k)}] \\ + h_{jr} \sum_{k=1}^{m} [p_k e^{(-\xi_j \omega_{nj} - j\omega_{dj})(t - T_k)}] \\ - j h_{jc} \sum_{k=1}^{m} [p_k e^{(-\xi_j \omega_{nj} - j\omega_{dj})(t - T_k)}]] \end{aligned} \tag{13}$$

Writing the complex exponential component as a function of sine and cosine, the response of a linear, time-invariant, with viscous damping, and multiple degrees of freedom system to a series of external step responses can be modelled by

$$x(t) = p_0 h_0 + \sum_{j=1}^{n}[2h_{jr}\sum_{k=1}^{m} p_k e^{(-\xi_j\omega_{nj})(t-T_k)}\cos(\omega_{dj}(t-T_k)) + 2h_{jc}\sum_{k=1}^{m} p_k e^{-\xi_j\omega_{nj}(t-T_k)}\sin(\omega_{dj}(t-T_k))] \quad (14)$$

The torsional vibrations with the natural frequency ω_{nj} are zero when the set of steps p_k at times T_k is orthogonal to the vibration mode. This condition is met when (15) is satisfied. This means that by choosing the step value p_k and the timing of the step connection T_k, as a function of the vibration modes frequency ω_{nj} and damping ξ_j, the excitation of torsional vibrations after the connection of electrical loads can be suppressed.

$$\sum_{k=1}^{m} p_k e^{-\xi_j\omega_{nj}T_k}\cos(\omega_d jT_k) = 0$$
$$\sum_{k=1}^{m} p_k e^{-\xi_j\omega_{nj}T_k}\sin(\omega_d jT_k) = 0 \quad (15)$$

This paper proposes a load connection pattern that solves (15) and can be applied to electrical loads in the MEA, such as the IPS. This kind of load pattern is known as input-shaping or Posicast compensator [24], [25]. Then, the open-loop compensator connects a load $f(t)$ as a series of pulses of values $p_k = (-1)^{k+1}$ at times T_k. The timing T_k of each segment of the load connection allow the elimination of the overshoot for systems with one or more natural frequencies, as given by (15). By solving (15) with $p_k = (-1)^{k+1}$, the excitation times T_k that suppress the vibrations are found.

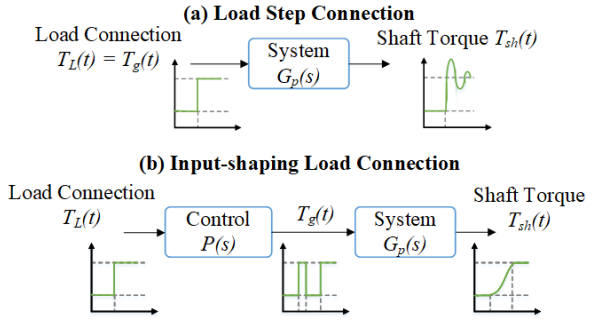

FIGURE 3. System control diagram and torque response. (a) Without input-shaping (b) With input-shaping.

Fig. 3 shows the expected transient response of a system after applying a step without and with the input-shaping strategy. In Fig. 3 (a), the load is connected as one step, while in Fig. 3 (b), the open-loop input-shaping load connection is applied, and consequently, torsional vibrations are not excited. In particular, Fig. 3 (b) considers the connection of resistive loads as a series of on/off switching pulses. This specific connection is applicable to aircraft loads, such as the IPS, where solid-state switches connect electrical loads.

Replacing the load pulsating pattern $p_k = (-1)^{k+1}$ into (15) and expanding the system for n natural frequencies, the following non-linear system is obtained.

$$\begin{bmatrix} \sum_{k=1}^{m}(-1)^{k+1}e^{-\xi_1\omega_{n1}T_k}\cos(\omega_{d1}T_k) \\ \sum_{k=1}^{m}(-1)^{k+1}e^{-\xi_1\omega_{n1}T_k}\sin(\omega_{d1}T_k) \\ \vdots \\ \sum_{k=1}^{m}(-1)^{k+1}e^{-\xi_n\omega_{nn}T_k}\cos(\omega_{dn}T_k) \\ \sum_{k=1}^{m}(-1)^{k+1}e^{-\xi_n\omega_{nn}T_k}\sin(\omega_{dn}T_k) \end{bmatrix} = 0 \quad (16)$$

The load connection times T_k are found considering $T_1 \leq T_2 \leq \ldots \leq T_k \leq \ldots \leq T_m$ and $T_1 = 0$. The number of steps for a system with n frequencies is given by $m = 2n + 1$. Being the system non-linear, it is not possible to provide a closed-form for its solutions, which are found employing offline numerical solver considering specific system parameters. In this work, OptiToolbox is used.

To analyze the behaviour of the proposed input-shaping strategy, a system with one natural frequency is firstly studied. In this case, for one natural frequency $n = 1$, three pulses are applied ($m = 3$) to suppress the torsional vibrations' excitation. To study the solutions of the method, the time connections are normalized by the period T_p and $\Gamma_k := T_k/T_p$ is defined. Likewise, the damping is redefined as $\delta := \xi/\sqrt{(1-\xi^2)}$. By substituting n, m, Γ_k and δ into (16) and considering that in the case of a single natural frequency $T_1 = 0$ and $\Gamma_1 = 0$, the following system is obtained:

$$\begin{bmatrix} 1 - e^{-2\pi\delta\Gamma_2}\cos(2\pi\Gamma_2) + e^{-2\pi\delta\Gamma_3}\cos(2\pi\Gamma_3) \\ -e^{-2\pi\delta\Gamma_2}\sin(2\pi\Gamma_2) + e^{-2\pi\delta\Gamma_3}\sin(2\pi\Gamma_3) \end{bmatrix} = 0 \quad (17)$$

To understand the behaviour of the proposed input-shaping method, Fig. 4 shows the solutions of the single equations in (17) for different damping ratios values ξ. In Fig. 4 (a) the solutions with $\xi = 0$ are shown, while in Fig. 4 (b) and (c) the cases with $\xi = 0.05$ and $\xi = 0.1$ are presented. The intersections (marked by *) of Γ_2, Γ_3 represent the solutions of the overall system in (17).

It can be observed that the system has multiple solutions, of which only one is within half a system period, $2\pi/\omega_d$, independently of the damping value ξ. For this reason, even if sets of load connection times longer than half a system period are also possible solutions to eliminate the excitation of torsional vibrations, the unique solution within half of the system period is applied. This solution is shown in Fig. 5 for different damping values. Thus, there is always a stable load connection in less than half the system period $2\pi/\omega_d$. Moreover, while the connection times Γ_2 and Γ_3 are evenly distributed in time for low values of ξ, their values get closer,

increasing ξ and, at the critical damping, $\xi = 1$, their values are equal. This shows that the input-shaping method is not needed in highly damped systems.

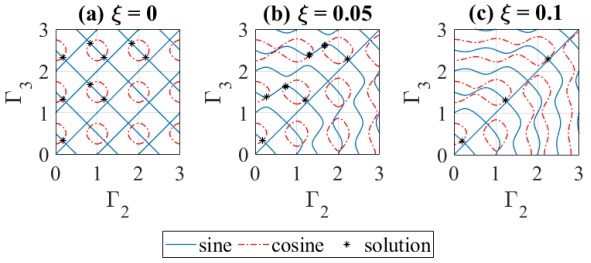

FIGURE 4. Solutions of the system in (17). Γ_2 (in blue) and Γ_3 (in red). (a) Solutions with no damping $\xi = 0$. (b) Solutions with damping $\xi = 0.05$, (c) Solutions with damping $\xi = 0.1$.

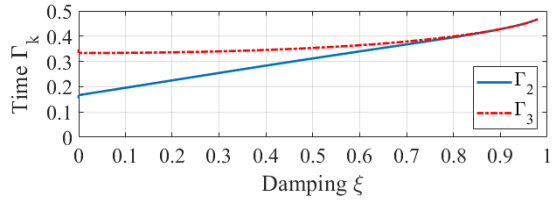

FIGURE 5. Time connection as a function of ξ. Γ_2 (in blue) and Γ_3 (in red).

IV. SIMULATION RESULTS

The electrical and mechanical parameters of the system of Fig. 2 are listed in 1. These values are selected to have natural frequencies close to a real aircraft drivetrain, as shown in [9]. To test the step connection and show the electromechanical interaction phenomena, a $R_L = 5\Omega$ resistive load is connected to the system in Fig. 2, when operating in steady state with a field current $i_f = 6.2A$ and $R_P = 60\Omega$. Fig. 6 shows the results obtained. In Fig. 6 (a) the armature (in blue) and field current (in red) are presented. In Fig. 6 (b), the armature (in blue) and field (in red) voltage are shown. In Fig. 6 (c), the speed is given, and in Fig. 6 (d), the torque applied by the machine (in red) and the shaft torque (in blue) are depicted.

As shown in Fig. 6 (b), v_a is not constant since it is not controlled. For this reason, the field current in Fig. 6 (a) and the field voltage in Fig. 6 (b) remain constant independently of the load R_{eq} connected. However, since T_g is proportional to i_a independently of v_a, the torque waveform and, consequently, its oscillations are not affected by armature voltage v_a variations. It can be noted that the load connection excites a damped oscillation in the drivetrain speed, as shown in Fig. 6 (c). This can be explained by looking at the torque at the generator shaft $T_{sh} = T_{6,7}$ and the torque applied by the machine T_g, as shown in Fig. 6 (d) in red. It can be observed that the transient torque response of T_{sh} in blue shows the excitation of torsional vibrations on the machine shaft, demonstrating the electromechanical interaction.

TABLE 1. Electrical and mechanical system's parameters.

Parameter	Value
Armature resistance	$R_a = 4.025\Omega$
Protection resistance	$R_P = 60\Omega$
Torque constant	$k = 0.1274$ Nm/A^2
Drop voltage brushes	$V_0 = 12.247$ V
Armature inductance	$L_a = 0.019$ H
Referred motor inertia	$J_1 = 0.0026$ Kgm^2
Referred motor flywheel inertia	$J_2 = 0.0172$ Kgm^2
Gears inertia	$J_{3,4,5,6} = 0.0151$ Kgm^2
Generator flywheel inertia	$J_7 = 0.0386$ Kgm^2
Generator inertia	$J_8 = 0.0005$ Kgm^2
Referred motor coupling stiffness	$k_{12} = 50403$ Nm/rad
Referred motor shaft stiffness	$k_{23} = 959.9111$ Nm/rad
Generator shaft stiffness	$k_{67} = 2239.8$ Nm/rad
Generator coupling stiffness	$k_{78} = 113406$ Nm/rad

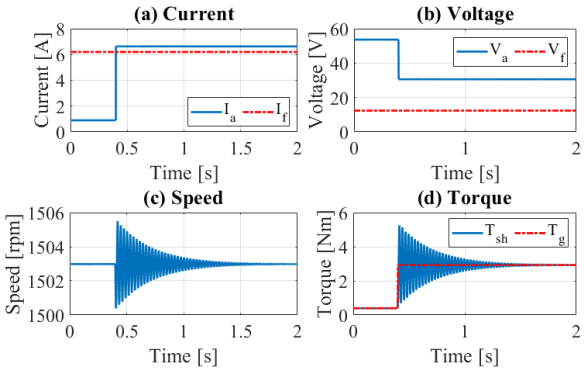

FIGURE 6. Simulation step response of the electromechanical system. (a) Machine armature (in blue) and field (in red) current (b) Machine armature (in blue) and field (in red) voltage (c) Machine Speed (d) Machine (in red) and shaft (in blue) torque.

To calculate the input-shaping load connection, the mechanical vibrations frequencies are obtained through Fast Fourier Transform (FFT) analysis of the shaft torque T_{sh} after the step connection. The results obtained are shown in Fig. 7. The Hilbert Transform Method combined with empirical mode decomposition (EMD) is used to determine the damping. The frequencies obtained are $f_1 = 36.00$ Hz, $\xi_1 = 0.0127$, $f_2 = 86.10$ Hz and $\xi_2 = 0.0194$.

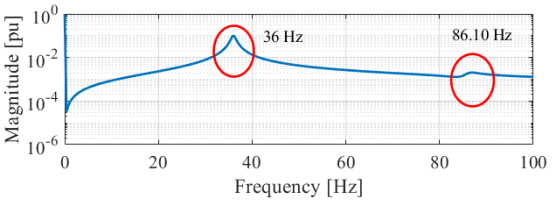

FIGURE 7. Shaft torque T_{sh} Fourier analysis after a load step connection.

By applying the input-shaping method, described in Section III, solved for the two drivetrain torsional modes ($f_1 = 36.00$ Hz, $\xi_1 = 0.0127$, and $f_2 = 86.10$ Hz, $\xi_2 = 0.0194$) of the system under study, the electromechanical interaction effects can be eliminated. Fig. 8 shows the results obtained for the electromechanical system operating with constant i_f when an electrical load R_L is connected

using the proposed method. Fig 8 (a) and Fig. 8 (b) show the system's voltages and currents, respectively. The field voltage and current are depicted in red, and the armature voltage and current in blue. It can be noted that using the proposed methodology, the load R_L is now connected in a series of pulses, of which the number and amplitude are found by solving the system of equation in (16), with $n = 2$ and $m = 5$. In Fig. 8 (c) and Fig. 8 (d) the system speed and generator torque T_g (in red) plus generator shaft torque $T_{sh} = T_{6,7}$ (in blue) are shown, respectively. The results show that the connection of the electrical load using the proposed input-shaping method cancels torsional vibrations, and the load is connected smoothly without torque or speed oscillations.

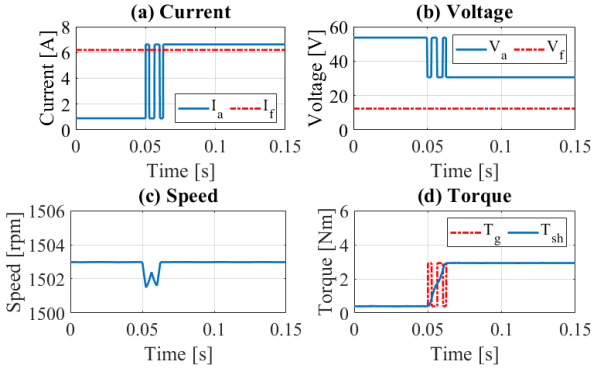

FIGURE 8. Simulation results with input-shaping open-loop control. (a) Machine armature (in blue) and field (in red) current (b) Machine armature (in blue) and field (in red) voltage (c) Machine Speed (d) Machine (in red) and shaft (in blue) torque.

Comparing Fig. 8 with the results obtained in Fig. 6, the use of the proposed input-shaping strategy allows the elimination of torsional vibrations after the sequence of pulsed connections has been applied to the system. This strategy is applied considering squared connections; hence, it can be applied to systems where the inductance is much smaller than the resistance. It is also clear that, when compared with other strategies found in the literature for reduction of torsional vibrations, such as ramp load connection and machine torque control, the input-shaping technique allows the reduction of the vibration in a minimal time. Since $T_5 = 12.544$ ms, the connection takes place in less than half a period of the drivetrain natural frequencies ($T_p/2 = 19.698$ ms), which is hardly achieved with other strategies. Moreover, in ramp connections, the proposed input-shaping strategy can still be applied, and a minimum connection time or optimal shape can be found.

Also, the frequencies excited in the shaft after the electrical load connection are analyzed, calculating the FFT to the shaft torque T_{sh}. The result obtained is shown in Fig. 9. When compared to Fig. 7, it can be noted the system resonance frequencies are suppressed, verifying that the use of the proposed input-shaping methodology suppresses the excitation of the mechanical natural frequencies.

Finally, to further study the proposed input-shaping method's behaviour and understand its effect on the system,

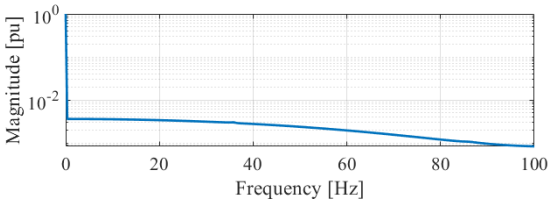

FIGURE 9. Shaft torque T_sh Fourier analysis after a load connection using the input-shaping control.

a zero-pole analysis is presented in Fig. 10. To obtain the zero-pole root locus, the transfer function of the system is calculated in the Laplace domain. The transfer function of the system with the compensator is given by:

$$H_{Sys}(s) = H_{IS}H_{Plant}(s) \tag{18}$$

In which, H_{plant} is the drivetrain transfer function obtained from the model obtained from (3), and H_{IS} is the input-shaping compensator, given by:

$$P(s) = e^{-sT_1} - e^{-sT_2} + e^{-sT_3} \tag{19}$$

In (19), the input-shaping control or Posicast compensator is modelled in the Laplace domain as a series of delayed step connections, with T_1,T_2, and T_3 the step connection times. Fig. 10 shows the poles (represented by x) and zeros (represented by o) of the drivetrain. It is observed that since the poles are in the left semi plane, the system is stable. Moreover, since the zeros added by the input-shaping compensator have the same value as the poles of the mechanical drivetrain, the excitation of the torsional vibrations is suppressed.

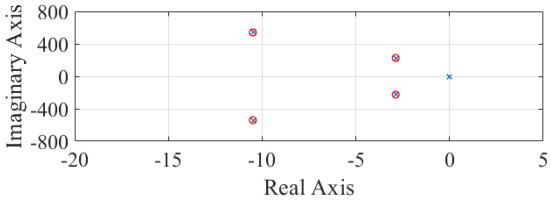

FIGURE 10. Poles (shown by x) and zeros (shown by o) of the system.

V. EXPERIMENTAL RESULTS

To experimentally validate the proposed solutions, the electromechanical system of Fig. 2 is built. The drivetrain, shown in Fig. 11 (a), is composed of a 2.2 kW, two-pole pair induction motor with a nominal speed of 1445 rpm and controlled using Volt/frequency control while a 1 kW Nidec Universal Motor is operated as an independent field DC generator. The electrical power system, shown in Fig. 11 (b), is composed of a resistance bank of $R_P = 60\Omega$, and a variable load resistance R_L. A CM225DX-24S1 IGBT with a Powerex VLA536-01R gate driver is used to connect and disconnect the load resistance R_L. The IGBT is controlled using an Infineon XE166FN microcontroller. The drivetrain mechanical system comprises two flywheels inertias designed to obtain the same torsional frequencies of simulation tests. The system

is designed considering the same parameters of the simulation shown in 1. The electrical signals, armature current i_a, armature voltage v_a, and field current i_f, are measured with LEM transducers and recorded using dSpace MicrolabBox. The torque is determined using the sensorless method presented in [9].

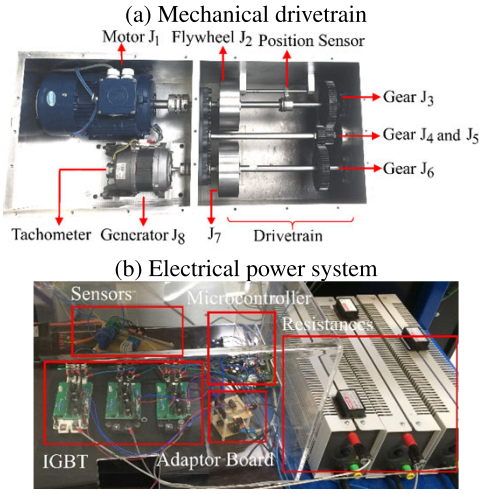

FIGURE 11. Experimental setup: (a) Mechanical drivetrain. (b) Electrical power system.

As presented in Section III, the proposed input-shaping method depends on the drivetrain's frequency and damping. The drivetrain torsional frequencies are verified to validate the mechanical system design, calculating the FFT after a step connection is applied to the system. Since the torque is measured using a sensorless method, the FFT is applied to the armature current, which is proportional to the torque as given by (4). The information recorded consists of 10 seconds of the armature current with a sampling frequency $f_s = 10$ kHz. Fig. 12 shows the normalized Fourier response of the system operating at 1500 rpm when the field current is 6.2 A, the initial load is 0.41 Nm, and the final load in the system is 2.92 Nm. In Fig. 12, the torsional frequencies of the drivetrain are highlighted in red. The obtained frequencies values are $f_1 = 35.5$ Hz and $f_2 = 77.1$ Hz, respectively. The Hilbert Transform Method, combined with empirical mode decomposition (EMD), is used to identify the damping ratio. The damping ratios obtained are $\xi_1 = 0.018$, and $\xi_2 = 0.012$, respectively. These values present minimal variation with respect to the simulated ones, shown in Fig. 7, making the simulation and experimental systems comparable. These differences are mainly related to parasitic parameters and tolerances of the manufactured mechanical system.

The connection of the load as a single step and using the proposed input-shaping method is verified under the following conditions: $i_f = 6.2$ A, $\omega_8 = 1550$ rpm, $R_P = 60\Omega$, and $R_L = 4.95\Omega$. In terms of power and torque, both tests' initial load values, using the step connection and the input-shaping strategy, are 50.82 W and 0.41 Nm. Likewise, the final load connected for each test is 210.52 W and 2.92 Nm. The connection times for the proposed input-shaping control are

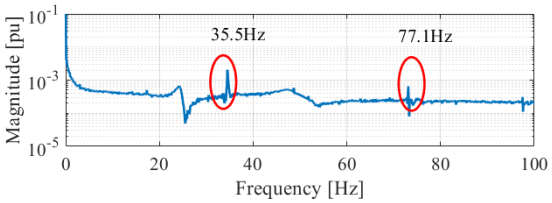

FIGURE 12. Fourier analysis of the experimental armature current at 1500 rpm after a load step connection.

TABLE 2. Load connection performance.

Connection	Overshoot [%]	Settling Time [s]
Step	80.85	0.64
Input-shaping	33.90	0.44

obtained, solving equation (16) for $n = 2$ and $m = 5$ and the frequencies and damping identified from the experimental analysis. The connection times obtained are: $T_1 = 0$ s, $T_2 = 2.5$ ms, $T_3 = 6.7$ ms, $T_4 = 11.1$ ms, and $T_5 = 13.4$ ms. Thus, the connection takes place under 13.4 ms, which is lower than the 14.08 ms of half a period of the mechanical drivetrain. Also, since the timing of the connection is in the order of milliseconds, the slew rate of the IGBT ($600V/\mu s$ obtained for 600 V from the datasheet data) does not affect the control strategy.

In Fig. 13, the results obtained connecting the load as a step (left side Fig. 13 (a), (c), (e)) and using the proposed pulsating input-shaping strategy (right side Fig. 13 (b), (d), (f)) are shown. In Fig. 13 (a) and Fig. 13 (b), the machine field (in red) and armature (in blue) currents for the step load connection and the load input-shaping connection are shown. In Fig. 13 (c) and Fig. 13 (d), both cases' armature voltage is presented. In Fig. 13 (e) and Fig. 13 (f), the torque applied by the machine T_g (in red) and the shaft torque T_{sh} (in blue) for both cases (without and with the strategy) are also shown. From Fig. 13 (e) and Fig. 13 (f), it is observed that the initial and steady-state torque for the single-step connection and the proposed pulsating input-shaping strategy are the same (0.41 Nm and 2.93 Nm, respectively), making the results comparable. Fig. 13 (e) shows that the single-step connection excites torsional vibrations in the shaft. These vibrations produce a peak torque of 5.2 Nm in the drivetrain shaft. Instead, the results obtained using the proposed input-shaping method in Fig. 13 (f) show that the compensator's use reduces the peak torque vibrations from 5.2 Nm to 3.9 Nm.

To analyze this further, 2 presents the overshoot and settling time (calculated for 5% of the steady-state torque value) when the load is connected as a step and using the proposed methodology. These results show that the input-shaping open-loop control reduces the overshoot by 50% and the settling time by 200 ms, extending the mechanical components' lifespan by decreasing the peak torque and reducing the vibration time.

When comparing the experimental and simulation results obtained in Fig. 6 and Fig. 13, it is observed that the

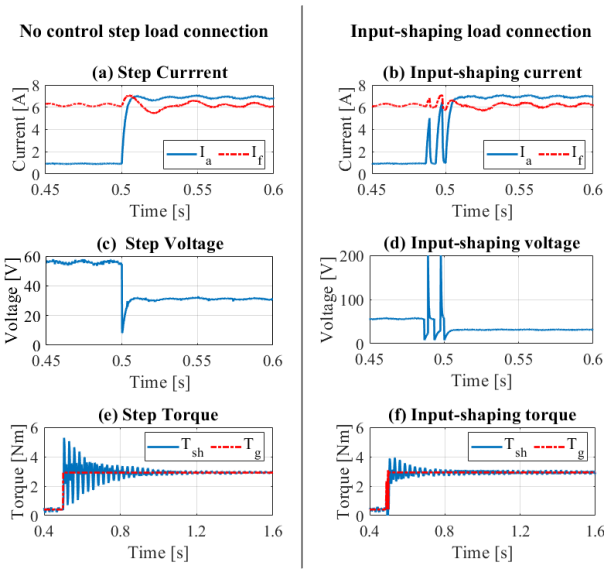

FIGURE 13. Experimental results without control strategy (Fig (a), (c), (e)) and with input-shaping (Fig (b), (c), and (d)). (a) and (b) Machine armature (in blue) and field (in red) current in step and input-shaping connection, respectively. (c) and (d) Machine armature voltage in step and input-shaping connection, respectively. (e) and (f) Machine (in red) and shaft (in blue) torque in step and input-shaping connection, respectively.

current, voltage, and torque obtained by simulation and experimentally presents similar values. Also, comparing the step connection torque of Fig. 13 (e) with the results obtained by simulation in Fig. 6, a similar behaviour is observed between the two the signal with the slight discrepancy clearly explained by the difference between resonance frequencies and damping values of the simulation and experimental model. Instead, comparing the torque obtained using the input-shaping control in Fig. 13 (f) with the simulation results in Fig. 8, it can be observed that while experimentally, the compensator is only able to reduce the torsional vibrations excited after the switching connection, in the simulation, the torsional vibrations are entirely eliminated. This difference is caused by the DC machine inductance, distorting the connection steps applied to the mechanical system, as seen from the armature current and voltage in Fig. 13 (b) and Fig. 13 (d). Moreover, the frequencies at which (16) was solved present a tolerance, and hence calculated connection times may present minor discrepancies from the one currently necessary to suppress the torsional vibrations. However, regardless of inductance and the uncertainty in the calculated frequencies, the experimental results show that the proposed methodology can reduce the torsional vibrations excited, regardless of the frequency uncertainty.

VI. CONCLUSION

This paper studies the reduction of torsional vibrations excited by the connection of electrical loads in an aircraft. To reduce the excitation of vibrations, an input-shaping control strategy implemented directly in the electrical loads was presented, theoretically analyzed, and experimentally validated.

Theoretical analysis of the input-shaping compensator shows that when the system is known and all components, such as inductances, are accounted for, the vibrations can be eliminated after the switching of the electrical load. This is based on the compensator's operation that suppresses the excitation of the torsional vibrations by cancelling the excitation of the mechanical system poles. Also, experimental results have shown that the proposed method effectively allows the reduction of the torsional vibrations excited by the connection of electrical loads by up to 50% of the maximum value obtained by a single step load connection.

Since the use of the proposed method allows the reduction of torsional vibrations even when frequencies uncertainty is present, as shown in the experimental results, the method is a suitable alternative to reduce the electromechanical interactions phenomena in aircraft systems. Also, for switching loads, such as IPS, the strategy can be directly applied, making its implementation straightforward and maintaining the required safety level and reliability necessary in aircraft systems.

In conclusion, using the proposed input-shaping methodology allows extending the mechanical components lifespan and the use of lighter weight generator shafts in aircraft applications, offering a solution for longer-lasting, more reliable MEA.

REFERENCES

[1] A. Barzkar and M. Ghassemi, "Electric power systems in more and all electric aircraft: A review," *IEEE Access*, vol. 8, pp. 169314–169332, 2020.
[2] ACARE, "Strategic research & innovation agenda," Advisory Council Aviation Res. Innov. Eur., Brussels, Belgium, Tech. Rep., 2017, vol. 1. [Online]. Available: https://www.acare4europe.org/sites/acare4europe.org/files/document/ACARE-Strategic-Research- Innovation-Volume-1.pdf
[3] P. W. Wheeler, J. C. Clare, A. Trentin, and S. Bozhko, "An overview of the more electrical aircraft," *Proc. Inst. Mech. Eng., G, J. Aerosp. Eng.*, vol. 227, no. 4, pp. 578–585, Apr. 2013. [Online]. Available: http://pig.sagepub.com/lookup/doi/10.1177/0954410012468538
[4] P. Wheeler, T. Samith Sirimanna, S. Bozhko, and K. S. Haran, "Electric/hybrid-electric aircraft propulsion systems," *Proc. IEEE*, vol. 109, no. 6, pp. 1115–1127, Jun. 2021.
[5] P. Wheeler, A. Trentin, S. Bozhko, and J. Clare, "Regeneration of energy onto an aircraft electrical power system from an electro-mechanical actuator," in *Proc. Elect. Syst. Aircr., Railway Ship Propuls. (ESARS)*, Oct. 2012, pp. 1–6.
[6] R. L. Steigerwald, G. W. Ludwig, and R. Kollman, "Investigation of power distribution architectures for distributed avionics loads," in *Proc. Power Electron. Spec. Conf. (PESC)*, vol. 1, Jun. 1995, pp. 231–237. [Online]. Available: http://ieeexplore.ieee.org/document/474817/
[7] B. Sarlioglu and C. T. Morris, "More electric aircraft: Review, challenges, and opportunities for commercial transport aircraft," *IEEE Trans. Transp. Electrific.*, vol. 1, no. 1, pp. 54–64, Jun. 2015. [Online]. Available: http://ieeexplore.ieee.org/document/7098414/
[8] T. Feehally, I. E. Damian, and J. M. Apsley, "Analysis of electromechanical interaction in aircraft generator systems," *IEEE Trans. Ind. Appl.*, vol. 52, no. 5, pp. 4327–4336, Sep. 2016. [Online]. Available: http://ieeexplore.ieee.org/document/7500101/
[9] C. Ahumada and P. Wheeler, "Modelling of reduced electromechanical interaction system for aircraft applications," *IET Electr. Power Appl.*, vol. 13, no. 7, pp. 1061–1070, Jul. 2019. https://digital-library.theiet.org/content/journals/10.1049/iet-epa.2019.0122
[10] G. Moore, "Electro-mechanical interactions in aerospace gas turbines," Ph.D. dissertation, Dept. Elect. Electron. Eng., Univ. Nottingham, Nottingham, U.K., 2013.

[11] M. H. Marzebali, S. H. Kia, H. Henao, G.-A. Capolino, and J. Faiz, "Planetary gearbox torsional vibration effects on wound-rotor induction generator electrical signatures," *IEEE Trans. Ind. Appl.*, vol. 52, no. 6, pp. 4770–4780, Nov. 2016. [Online]. Available: http://ieeexplore.ieee.org/document/7544611/

[12] J. Kavil Kambrath, Y. Wang, Y.-J. Yoon, A. Aaron Alexander, X. Liu, G. Wilson, C. J. Gajanayake, and A. K. Gupta, "Modeling and control of marine diesel generator system with active protection," *IEEE Trans. Transp. Electrific.*, vol. 4, no. 1, pp. 249–271, Mar. 2018. [Online]. Available: http://ieeexplore.ieee.org/document/8070961/

[13] L. Ran, D. Xiang, and J. L. Kirtley, "Analysis of electromechanical interactions in a flywheel system with a doubly fed induction machine," *IEEE Trans. Ind. Appl.*, vol. 47, no. 3, pp. 1498–1506, May 2011. [Online]. Available: http://ieeexplore.ieee.org/document/5729815/

[14] M. A. Valenzuela, J. M. Bentley, and R. D. Lorenz, "Evaluation of torsional oscillations in paper machine sections," *IEEE Trans. Ind. Appl.*, vol. 41, no. 2, pp. 493–501, Mar./Apr. 2005. [Online]. Available: http://ieeexplore.ieee.org/document/1338357/ and [Online]. Available: http://ieeexplore.ieee.org/document/1413513/

[15] C. Wang, M. Yang, W. Zheng, J. Long, and D. Xu, "Vibration suppression with shaft torque limitation using explicit MPC-PI switching control in elastic drive systems," *IEEE Trans. Ind. Electron.*, vol. 62, no. 11, pp. 6855–6867, Nov. 2015. [Online]. Available: http://ieeexplore.ieee.org/document/7113842/

[16] J. K. Kambrath, C. Yoon, J. Mathew, X. Liu, Y. Wang, C. J. Gajanayake, A. K. Gupta, and Y.-J. Yoon, "Mitigation of resonance vibration effects in marine propulsion," *IEEE Trans. Ind. Electron.*, vol. 66, no. 8, pp. 6159–6169, Aug. 2019. [Online]. Available: https://ieeexplore.ieee.org/document/8495022/

[17] J. Kavil Kambrath, M. S. U. Khan, Y. Wang, A. I. Maswood, and Y.-J. Yoon, "A novel control technique to reduce the effects of torsional interaction in wind turbine system," *IEEE J. Emerg. Sel. Topics Power Electron.*, vol. 7, no. 3, pp. 2090–2105, Sep. 2019.

[18] G. Mandic, A. Nasiri, E. Muljadi, and F. Oyague, "Active torque control for gearbox load reduction in a variable-speed wind turbine," *IEEE Trans. Ind. Appl.*, vol. 48, no. 6, pp. 2424–2432, Nov. 2012.

[19] I. U. Khan and R. Dhaouadi, "Robust control of elastic drives through immersion and invariance," *IEEE Trans. Ind. Electron.*, vol. 62, no. 3, pp. 1572–1580, Mar. 2015. [Online]. Available: http://ieeexplore.ieee.org/lpdocs/epic03/wrapper.htm?arnumber=6928460

[20] Y. Wang, Q. Zheng, H. Zhang, and L. Miao, "Adaptive control and predictive control for torsional vibration suppression in helicopter/engine system," *IEEE Access*, vol. 6, pp. 23896–23906, 2018. [Online]. Available: https://ieeexplore.ieee.org/document/8351981/

[21] M. Yang, C. Wang, D. Xu, W. Zheng, and X. Lang, "Shaft torque limiting control using shaft torque compensator for two-inertia elastic system with backlash," *IEEE/ASME Trans. Mechatronics*, vol. 21, no. 6, pp. 2902–2911, Dec. 2016. [Online]. Available: http://ieeexplore.ieee.org/document/7475935/

[22] J. Licari, C. E. Ugalde-Loo, J. B. Ekanayake, and N. Jenkins, "Damping of torsional vibrations in a variable-speed wind turbine," *IEEE Trans. Energy Convers.*, vol. 28, no. 1, pp. 172–180, Mar. 2013. [Online]. Available: http://ieeexplore.ieee.org/document/6361459/

[23] L. Liu and D. Xie, "Performance comparison of two different filter design approaches for torsional vibration damping in a doubly fed induction generator-based wind turbine," *J. Eng.*, vol. 2015, no. 6, pp. 197–204, Jun. 2015. [Online]. Available: http://digital-library.theiet.org/content/journals/10.1049/joe.2015.0029 and [Online]. Available: https://onlinelibrary.wiley.com/doi/10.1049/joe.2015.0029

[24] T. Singh, *Optimal Reference Shaping for Dynamical Systems*. New York, NY, USA: CRC Press, Oct. 2010. [Online]. Available: https://www.taylorfrancis.com/books/9781439805633

[25] G. Tallman and O. Smith, "Analog study of dead-beat posicast control," *IRE Trans. Autom. Control*, vol. 4, no. 1, pp. 14–21, Mar. 1958. [Online]. Available: http://ieeexplore.ieee.org/lpdocs/epic03/wrapper.htm?arnumber=1104844

[26] J. Y. Hung, "Feedback control with posicast," *IEEE Trans. Ind. Electron.*, vol. 50, no. 1, pp. 94–99, Feb. 2003. [Online]. Available: http://ieeexplore.ieee.org/lpdocs/epic03/wrapper.htm?arnumber=1174064

[27] B. Boukhezzar and H. Siguerdidjane, "Nonlinear control of a variable-speed wind turbine using a two-mass model," *IEEE Trans. Energy Convers.*, vol. 26, no. 1, pp. 149–162, Mar. 2011.

CONSTANZA AHUMADA (Member, IEEE) received the B.Sc. and M.Sc. degrees in electrical engineering from the University of Chile, Santiago, Chile, in 2011 and 2013, respectively, and the Ph.D. degree in electrical and electronic engineering from the University of Nottingham, Nottingham, U.K., in 2018. Since 2018, she has been an Assistant Professor with the Department of Electrical Engineering, University of Chile. Her current research interests include electromechanical interaction and control strategies for the reduction of vibrations in aerospace and marine systems and wind turbines.

PATRICK WHEELER (Fellow, IEEE) received the B.Eng. degree (Hons.) and the Ph.D. degree in electrical engineering for his work on matrix converters from the University of Bristol, U.K., in 1990 and 1994, respectively. In 1993, he moved to the University of Nottingham, where he worked as a Research Assistant with the Department of Electrical and Electronic Engineering. In 1996, he became a Lecturer with the Power Electronics, Machines and Control Group, University of Nottingham, U.K., where he has been a Full Professor, since January 2008. He was the Head of the Department of Electrical and Electronic Engineering, University of Nottingham, from 2015 to 2018. He is currently the Head of the Power Electronics, Machines and Control Research Group, the Global Director of the University of Nottingham's Institute of Aerospace Technology, and the Li Dak Sum Chair Professor in electrical and aerospace engineering. He is also the IEEE PELS Vice-President for Technical Operations. He has published over 750 academic publications in leading international conferences and journals. He is a member of the IEEE PELs AdCom.